Available online at www.sciencedirect.com
ScienceDirect
International Journal of Thermal Sciences 46 (2007) 199–211
International Journal of Thermal Sciences
www.elsevier.com/locate/ijts

Numerical investigation of fluid flow and heat transfer over louvered fins in compact heat exchanger

V.P. Malapure, Sushanta K. Mitra *, A. Bhattacharya

Department of Mechanical Engineering, Indian Institute of Technology Bombay, Mumbai, 400076, India

Received 18 August 2005; received in revised form 20 April 2006; accepted 21 April 2006

Available online 5 June 2006

Abstract

Numerical investigation of fluid flow and heat transfer characteristics over louvered fins and flat tube in compact heat exchangers is presented in this study. Three-dimensional simulations of single and double row tubes with louvered fins have been conducted. Simulations are performed for different geometries with varying louver pitch, louver angle, fin pitch and tube pitch and for different Reynolds number. Conjugate heat transfer and conduction through the fins are considered. The air-side performance of heat exchanger is evaluated by calculating Stanton number and friction factor. The results are compared with experiment and a good agreement is observed. The local Nusselt number variation along the top surface of the louver is calculated and effects of geometrical parameters on the average heat transfer coefficient is computed. Design curves are obtained which can used to predict the heat transfer and the pressure drop for a given louver geometry.

Keywords: Friction factor; Heat exchangers; Louvered fins; Stanton number

1. Introduction

In compact heat exchangers, thermal resistance is generally dominant on the air-side and may account for 80% or more of the total thermal resistance. The air-side heat transfer surface area is 8 to 10 times larger than the water-side. However, given that the heat transfer coefficient of the water-side is 40 to 50 times higher than the air-side, the thermal resistance on the air-side turns out to be higher by a factor of 5 to 10. Any improvement in the heat transfer on air-side therefore improves the overall performance of the heat exchanger. One way to achieve such an enhancement is through the use of louvered fins as shown in Fig. 1. The louvers act to interrupt the air flow and create a series of thin boundary layers which have lower thermal resistance. Numerous experiments [1–4] have been performed to predict the overall air-side heat transfer coefficient and pressure drop in louvered fin heat exchangers with flat tube.

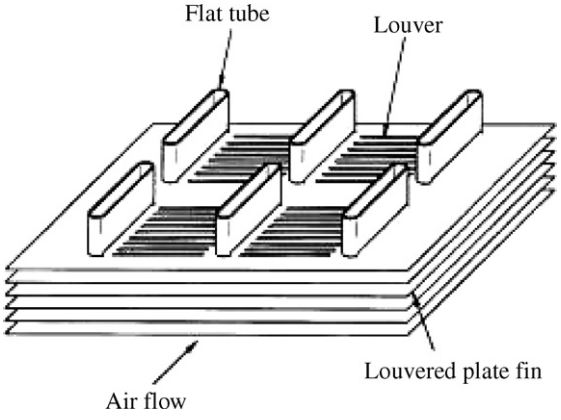

Fig. 1. Flat-sided tube and louvered plate fin heat exchanger [6].

Recently, generalized heat transfer and friction factor correlations have been proposed by Chang and Wang [5] and Chang et al. [6] for louvered fin geometry. The basic phenomenon in the louvered fin heat exchangers has been confirmed experimentally by Davenport [2], which is similar to Beauvais [7], by using smoke traces on scaled-up model of a non-standard variant of the louvered fin. They showed that the flow is mainly

* Corresponding author.
E-mail address: skmitra@me.iitb.ac.in (S.K. Mitra).

1290-0729/$ – see front matter
doi:10.1016/j.ijthermalsci.2006.04.010

Nomenclature

A	total heat transfer area
Ac	minimum flow area
c_p	specific heat at constant pressure
$C_{1\varepsilon}, C_{2\varepsilon}, C_\mu$	turbulence model constant
d_h	hydraulic diameter
f	friction factor
F_p	fin pitch
G_k	turbulent kinetic energy generation term
h	specific enthalpy
h_c	heat transfer coefficient
k	turbulent kinetic energy
L_p	louver pitch
L_s	fin length
$LMTD$	logarithmic mean temperature difference
n	number of rows
p	pressure
Q	heat transfer rate
Re_d	Reynolds number based on hydraulic diameter
Re_{Lp}	Reynolds number based on louver pitch
R_ε	rate of strain
S	modulus of mass rate of stress tensor
St	Stanton number
T	temperature
T_p	tube pitch
u	fluid velocity
U	mean velocity through minimum flow area

Greek symbols

α	louver angle
α_p	inverse Prandtl number
ΔT_i	temperature difference $T_{f,i}^{aw} - T_{a,i}$
ΔT_o	temperature difference $T_{f,o}^{aw} - T_{a,o}$
ρ	density
τ	stress tensor
ε	turbulent energy dissipation rate
μ	dynamic viscosity
λ	thermal conductivity

Subscript

a	air
eff	effective
f	fin
i	inlet
k	turbulent kinetic energy
o	outlet
t	turbulent

Superscript

aw	area weighted average

in the direction of fin at low Reynolds number but tends to get aligned with the louvers at higher Reynolds number. Davenport [2] and Achaichia and Cowell [1] investigated air-side heat transfer and flow behavior for louvered fin heat exchangers and presented the Stanton number and friction factor as a function of Reynolds number.

Wong and Smith [8] conducted experimental studies on large-scale models using hot-wire anemometer. They measured the overall drag coefficient and Nusselt number for a scaled model and found that the values agreed with those for an actual-size heat exchanger operating at same Reynolds number. Antoniou et al. [9] performed hot-wire measurements of mean velocity and r.m.s. velocity fluctuation in a scaled-up model, and showed that the flow remains laminar and steady for Re_{Lp} (Reynolds number based on louver pitch) up to 1300. For $Re_{Lp} > 1300$, the velocity fluctuates downstream of first one or two louvers. Kajino and Hiramatsu [10] and Webb and Trauger [11] used dye-line flow visualization technique to investigate the relationship between the flow alignment and geometrical parameters. They also found that the flow remains laminar and steady for Re_{Lp} up to 1300. Aoki et al. [12] performed an experimental study on heat transfer characteristics of different louver fin arrays and reported a decrease in heat transfer coefficient at low air velocities with increasing fin pitch. They also found that the heat transfer coefficient initially increases with louver angle reaching a maximum value at an angle of 28–30° after which it decreases.

Tafti et al. [13] studied the detailed transition mechanism from steady to unsteady flow in a multilouvered fin geometry. They found that initial instability appears in the wake of the exit louver at a Reynolds number (Re_{Lp}) of 400 and propagates inside the array as the Reynolds number is increased. Tafti and Zhang [14] studied the geometrical effects on flow transition in multilouvered fins. They found that instabilities are first developed in the wake of exit louver, which then spreads upstream into the louver bank. They also showed that the interior louver bank instabilities are completely independent of exit wake instability and the exit wake instability not only depends on the exit louver geometry, but it also depends on the upstream geometry of the louver bank. They found that louver angle and louver thickness have the largest effect on the onset of the exit wake and internal louver bank instabilities.

Cui and Tafti [15] conducted computational study of flow and heat transfer in a three-dimensional multilouvered fin. They found that the heat transfer is large in the transition region. Due to the flat landing of the louvers, 50 percent improvement in the tube surface heat transfer is achieved compared to the angled louver that extends to the tube surface. In spite of this high heat transfer in the transition region, the overall effect on louver mean heat transfer is small because of small spatial extent of the transition region. Tafti and Cui [16] performed three-dimensional simulations to investigate the fin-tube junction effects on flow and heat transfer in flat tube multilouvered heat exchangers. They found that the flow acceleration has a large impact on louver heat transfer locally. However, its impact is

minimal on the averaged heat transfer coefficient over the whole louver. They suggested to keep the transition and flat landing as small as possible for the best louver heat transfer performance. Perrotin and Clodic [17] conducted two- and three-dimensional numerical study of compact louvered heat exchangers for the determination of heat transfer and pressure drop characteristics. They found that the two-dimensional models over predict the heat transfer coefficient by up to 80 percent and the heat transfer coefficient calculated with three-dimensional models is much closer to the experimental data. Similar behaviour is also observed by Atkinson et al. [18].

Due to involvement of large number of geometrical parameters (e.g. louver pitch, louver angle, tube pitch, fin pitch, fin length) experimental studies are costly and time consuming to obtain the optimum configuration of heat exchanger. Hence, numerical studies are probably a more viable option for conducting a parametric study and investigating the effects of various parameters [10,18–20]. Springer and Thole [21] conducted both numerical and experimental studies on the flow behavior of louvered fin configuration and reported that the flow is louver directed for Reynolds number greater than 230. Tafti et al. [22] conducted a numerical investigation of the flow and temperature fields for two-dimensional louvered fin geometries and compared their results with experimental results of Achaichia and Cowell [1]. Suga and Aoki [12] in their numerical work studied the effects of louver angle, fin pitch and fin thickness on overall heat transfer performance and pressure drop. They presented values of overall Nusselt number and pressure drop for a wide range of geometrical parameters and Reynolds number. However their results are not validated by experiments. Mostly, two-dimensional numerical study of louvered fin is available in literature. These studies are based on the assumption of isothermal condition of the whole fin surfaces and neglecting thermal resistance of fins.

The present study numerically investigates the three-dimensional flow and heat transfer over louvered fins in compact heat exchangers considering conjugate heat transfer and fin resistance. The computational results are compared with experimental data by Achaichia and Cowell [1].

2. Governing equations

In this study, simulations are performed for Reynolds numbers (Re_d), which is based on hydraulic diameter, ranging from 400 to 4000. This is equivalent to Reynolds number range based on louver pitch (Re_{Lp}) of 60 to 1800. As outlined in the previous section, experimental observations of Antoniou et al. [9] have shown that the flow is laminar for up to a Reynolds numbers of approximately 1300. Even though flow unsteadiness occurs upstream and downstream of the louver for $Re_{Lp} = 1300$, the flow remains primarily laminar. To address this issue, three-dimensional simulations are performed in the current study with the RNG k–ε turbulence model in order to estimate the heat transfer and pressure drop characteristics and to verify the local turbulence behavior of the flow field. The heat transfer results are found to be 6–7% higher than those without turbulence model. Since this variation is not too large, the assumption of laminar flow is retained for Re_{Lp} up to 1300. For $Re_{Lp} > 1300$, the turbulent flow equations are solved. The governing equations representing the conservation of mass, momentum and energy are as follows:

In all of the equations, repeated subscripts denote summation.

- Mass conservation

$$\frac{\partial}{\partial x_j}(\rho u_j) = 0 \tag{1}$$

- Momentum conservation

$$\frac{\partial}{\partial x_j}(\rho u_j u_i - \tau_{ij}) = -\frac{\partial p}{\partial x_i} \tag{2}$$

where, τ_{ij} is the viscous stress tensor defined as,

$$\tau_{ij} = 2\mu S_{ij} - \frac{2}{3}\mu \frac{\partial u_k}{\partial x_k}\delta_{ij} \tag{3}$$

$$S_{ij} = \frac{1}{2}\left(\frac{\partial u_i}{\partial x_j} + \frac{\partial u_j}{\partial x_i}\right) \tag{4}$$

- Energy conservation

The energy equation solved in fluid domain is given by

$$\frac{\partial}{\partial x_j}\left(\rho u_j h - k\frac{\partial T}{\partial x_j}\right) = u_j \frac{\partial p}{\partial x_j} + \tau_{ij}\frac{\partial u_i}{\partial x_j} \tag{5}$$

and the energy equation solved in solid domain is given by

$$\frac{\partial}{\partial x_j}\left(\lambda \frac{\partial T}{\partial x_j}\right) = 0 \tag{6}$$

The effect of turbulence on the flow field is included through the application of RNG k–ε turbulence model, which is derived from the instantaneous Navier–Stokes equations, using a mathematical technique called renormalization group (RNG) methods.

- Kinetic energy

$$\frac{\partial}{\partial x_i}(\rho k u_i) = \frac{\partial}{\partial x_j}\left(\alpha_p \mu_{eff}\frac{\partial k}{\partial x_j}\right) + G_k - \rho\varepsilon \tag{7}$$

- Dissipation rate

$$\frac{\partial}{\partial x_i}(\rho \varepsilon u_i) = \frac{\partial}{\partial x_j}\left(\alpha_p \mu_{eff}\frac{\partial \varepsilon}{\partial x_j}\right) + C_{1\varepsilon}\frac{\varepsilon}{k}G_k - C_{2\varepsilon}\rho\frac{\varepsilon^2}{k} - R_\varepsilon \tag{8}$$

where, $\mu_{eff} = \mu + \mu_t$ and $\mu_t = \rho C_\mu \frac{k^2}{\varepsilon}$ in high Reynolds number range, $C_\mu = 0.0845$. Turbulent kinetic energy generation term is $G_k = 2\mu_t S^2{}_{ij}$.

The rate of strain term R_ε is given by

$$R_\varepsilon = \frac{C_\mu \rho \eta^3 (1 - \frac{\eta}{\eta_0})}{1 + \beta\eta^3}\frac{\varepsilon^2}{k} \tag{9}$$

where $\eta = \frac{Sk}{\varepsilon}$ and $\eta_0 = 4.38$ and $\beta = 0.012$. The RNG theory provides values of the turbulence constants $C_{1\varepsilon} = 1.42$ and $C_{2\varepsilon} = 1.68$, respectively.

The change in air temperature over the length of the fin is small, hence all properties of air can be assumed to be

constant and evaluated at the mean temperature. For the three-dimensional steady state model, conjugate heat transfer is taken into account. All thermo-physical properties of the tubes and fins surfaces are assumed to be constant.

3. Geometrical details

The dimensional details of louvered fin geometry considered for the analysis is shown in Fig. 2. The louvers are inclined in opposite directions for each tube row. At the inlet, outlet and intermediate section half-louver is used. Different combinations of fin pitch (Fp), louver pitch (Lp), tube transverse pitch (Tp) and louver angle (α) were used to conduct a parametric study. The values of these parameters are listed in Table 1 and are in accordance with the geometries reported in [1]. The finite thickness of the copper fin for all configurations is taken to be 0.05 mm, the tube size as 16×2 mm, the longitudinal tube pitch as 20 mm and the length of the fins in the airflow direction as 21.6 mm for single row and 41.6 mm for double row tubes. The three-dimensional computational domain, as shown in Fig. 3, consists of single fin with top and bottom as a periodic boundary. The geometry is simplified compared to the actual louver fin geometry to avoid the highly skewed element which will create solution convergence issue. This simplification has some impact on fin temperature distribution but the effect on overall heat transfer rate is minimal. To reduce the computational mesh size, one half of the fin height is considered with symmetry boundary condition.

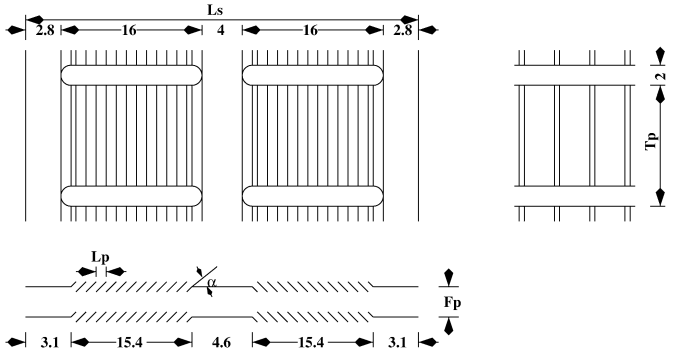

Fig. 2. Three views of louvered fins (dimensions are in mm).

4. Computational details

The commercial code FLUENT 6.1 [23] is used for the numerical solution of the Navier–Stokes and energy equations. FLUENT uses a control-volume-based technique to convert the governing equations to algebraic equations that can be solved numerically. This involves subdividing the region in which the flow is to be solved into individual cells or control volumes so that the equations can be integrated numerically on a cell-by-

Table 1
Dimensional details of computational geometry.

Configuration No.	F_p [mm]	L_p [mm]	α [°]	T_p [mm]	n	d_h [mm]
1	2.02	1.4	25.5	11	2	3.33
2	3.25	1.4	25.5	11	2	4.97
3	1.65	1.4	25.5	11	2	2.78
4	2.09	1.4	21.5	11	2	3.43
5	2.03	1.4	28.5	11	2	3.34
6	2.15	1.4	25.5	11	1	3.50
7	1.70	1.4	25.5	11	1	2.84
8	2.11	0.81	29	11	2	3.43
9	1.72	0.81	29	11	2	2.86
10	3.33	0.81	29	11	2	5.03
11	2.18	1.1	30	11	2	3.55
12	2.16	0.81	20	11	2	3.50
13	2.16	1.1	28	8	2	3.27
14	2.17	1.1	22	14	2	3.67
15	2.17	1.1	22	8	2	3.29

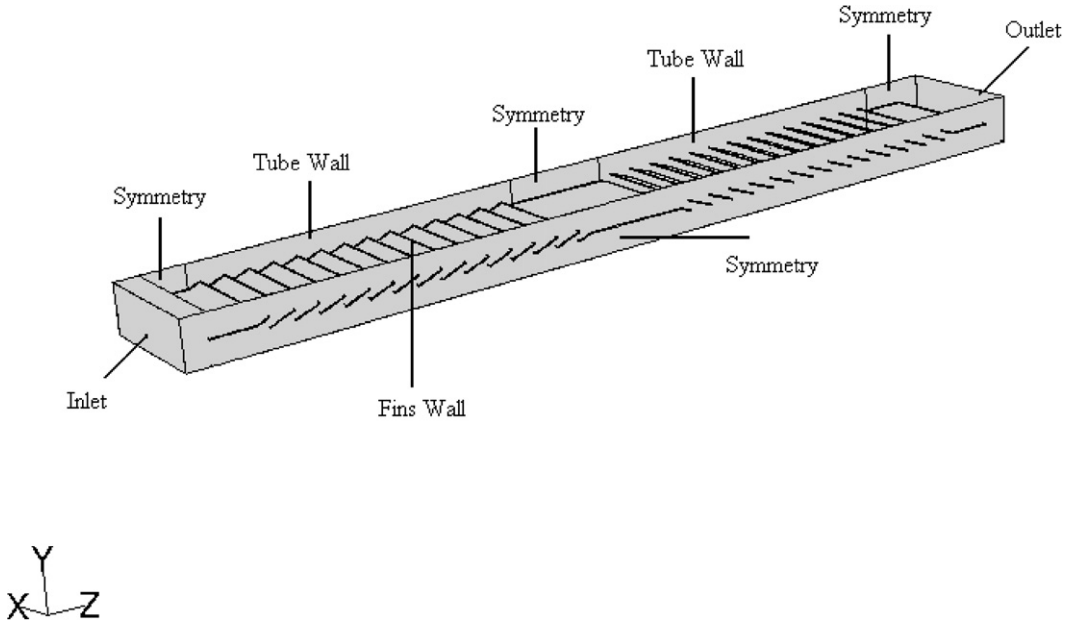

Fig. 3. 3-D computational domain.

cell basis to produce discrete algebraic (finite volume) equations [24,25]. All variables, including velocity components, pressure and temperature, are averages applied to a control volume. A second-order spatial interpolation method is employed to obtain the velocity components, pressure and temperature on the control volume faces from those at the control volume centers. The control volume face values of the dependent variables are used to evaluate the convective fluxes.

Fluent's segregated steady-state solver is used for the numerical simulations. The SIMPLE algorithm is used to couple pressure and velocity. A second-order upwind scheme is used for the space discretization of the momentum, turbulence and energy equations in the simulations. Also, a second-order accurate scheme is used to interpolate the pressure value on the control volume faces from those at the control volume centers in the momentum equations. The under-relaxation factors for the update of computed variables at each iteration are for pressure = 0.3, momentum = 0.7, turbulence kinetic energy = 0.8, turbulence dissipation rate = 0.8 and energy = 1. The residuals of the continuity, components of velocities, turbulent kinetic energy and turbulent dissipation rate are below 10^{-5}, while for energy it is below 10^{-7} for converged solution.

The HEX/WEDGE mesh is generated using Gambit, the meshing tool packaged with FLUENT CFD software. The grid independence is checked using two different mesh size. For coarse mesh, cell size equal to fin thickness is used and for fine mesh, cell size is half of the fin thickness. It is found that the variation in solutions are within 2–3%. The average skewness for this mesh is 0.1 with maximum skewness of 0.4.

Due to symmetry of the flow domain, calculations are performed for half fin height and periodic conditions are imposed on the top and bottom of the domain. At the inlet, velocity boundary is imposed, in which uniform velocity magnitude and temperature of air are defined by user. For turbulent flow, turbulent intensity is defined as per correlation suggested in Fluent User's manual $I = 0.16Re_d^{-1/8}$. The pressure-outlet boundary is used at outlet plane, where static gauge pressure and temperature are given. Tubes walls are defined as constant wall temperature. On the fin and tube surfaces, no slip boundary condition is assumed to exist.

5. Calculation of performance parameters

The performance of compact heat exchanger depends on the geometry and flow conditions. For a given set of conditions, the pressure drop and heat transfer performance of louvered fin can be characterized by a friction factor and Stanton number, respectively. The geometric condition can be characterized in terms of dimensionless parameters such as fin-to-louver pitch ratio (F_p/L_p) and louver angle (α), while the flow condition can be characterized by Reynolds number. The conventions used by Kays and London [26] are followed throughout the calculations. The Reynolds number based on hydraulic diameter and louver pitch can be defined as

$$Re_d = \frac{\rho U d_h}{\mu}; \qquad Re_{Lp} = \frac{\rho U L_p}{\mu}; \qquad d_h = \frac{4A_c L_s}{A} \tag{10}$$

The friction factor and Stanton number are defined in terms of the total heat transfer area A, the minimum flow area A_c, and the mean velocity U through the minimum flow area, are given by:

$$f = \frac{\Delta p}{\frac{\rho U^2}{2}\frac{A}{A_c}} \tag{11}$$

$$St = \frac{h_c}{\rho U c_p} \tag{12}$$

where, the heat transfer coefficient h_c is defined in terms of the heat transfer rate Q and the logarithmic mean temperature difference *LMTD*:

$$h_c = \frac{Q}{A \times LMTD} \tag{13}$$

and

$$LMTD = \frac{\Delta T_o - \Delta T_i}{\ln(\Delta T_o/\Delta T_i)} \tag{14}$$

and the heat transfer rate is given by:

$$Q = \rho U A_c c_p (T_{a,o} - T_{a,i}) \tag{15}$$

Here, $\Delta T_i = T_{f,i}^{aw} - T_{a,i}$ and $\Delta T_o = T_{f,o}^{aw} - T_{a,o}$ and the superscript "*aw*" refers to the area weighted average temperature. Hence, the heat transfer coefficient and Stanton number can be defined as follows:

$$h_c = \rho U c_p \frac{A_c}{A}\frac{(T_{a,o} - T_{a,i})}{LMTD} \tag{16}$$

$$St = \frac{A_c}{A}\frac{(T_{a,o} - T_{a,i})}{LMTD} \tag{17}$$

6. Results and discussions

Numerical simulations were conducted for the described geometry of flat-sided tube and louvered plate fins. The louver pitch, louver angle, fin pitch and tube pitch were varied for $400 \leqslant Re_d \leqslant 4000$. Temperatures of the tube surface and inlet air were maintained at 358 K and 288 K, respectively. The results are presented in the form of velocity and temperature contours, streamlines, Stanton number and friction factor plots against Reynolds number.

6.1. Flow phenomena

The computed velocity and temperature contours for two different Reynolds numbers are shown in Figs. 4–7, respectively. It can be observed that at low Reynolds number, most of the air flows through the gap between the fins rather than through the louvers. This can be attributed to the high flow resistance presented by the louvers. At lower Reynolds number, since the air has less kinetic energy, most of it passes through the path of least resistance, i.e., through the fin gaps. The air temperature reaches the fin temperature in the second half of the louvered array, and as a result the heat transfer performance of the fin is poor. At low Reynolds number, second half of the louvers array only accounts for pressure loss without any significant

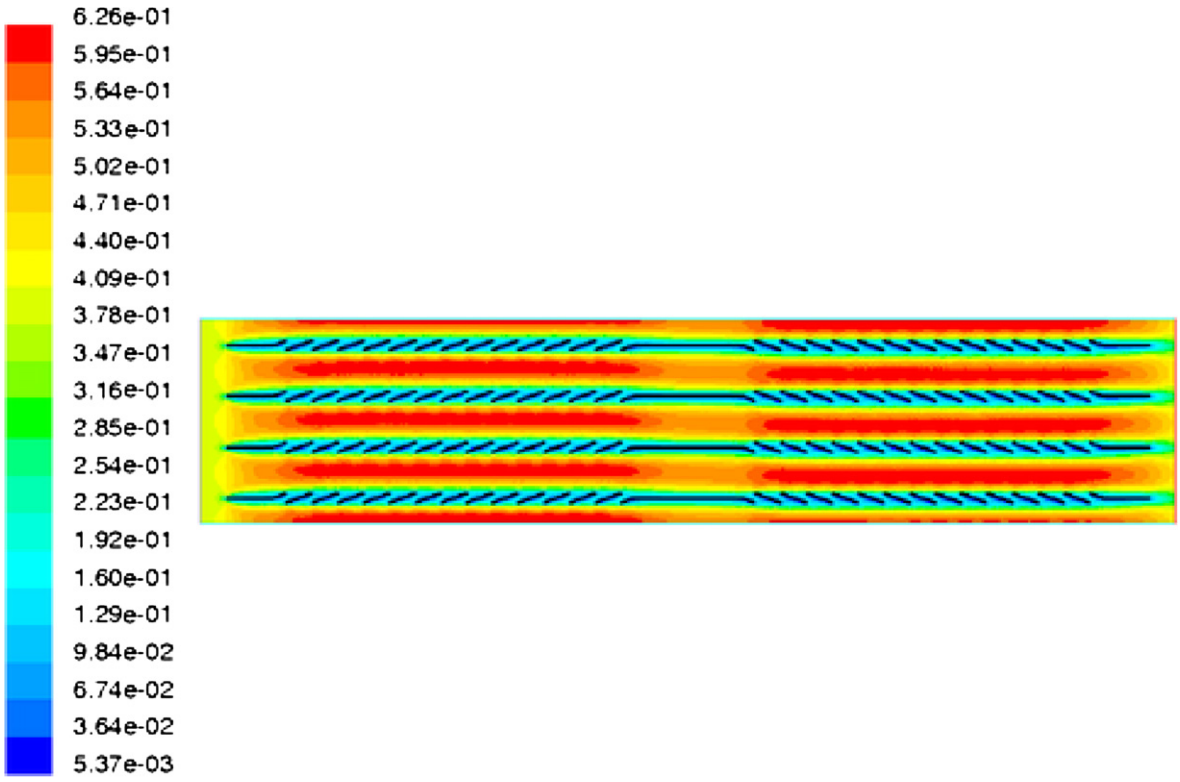

Fig. 4. Computed velocity ($\mathrm{m\,s^{-1}}$) contours for $Re_d = 100$.

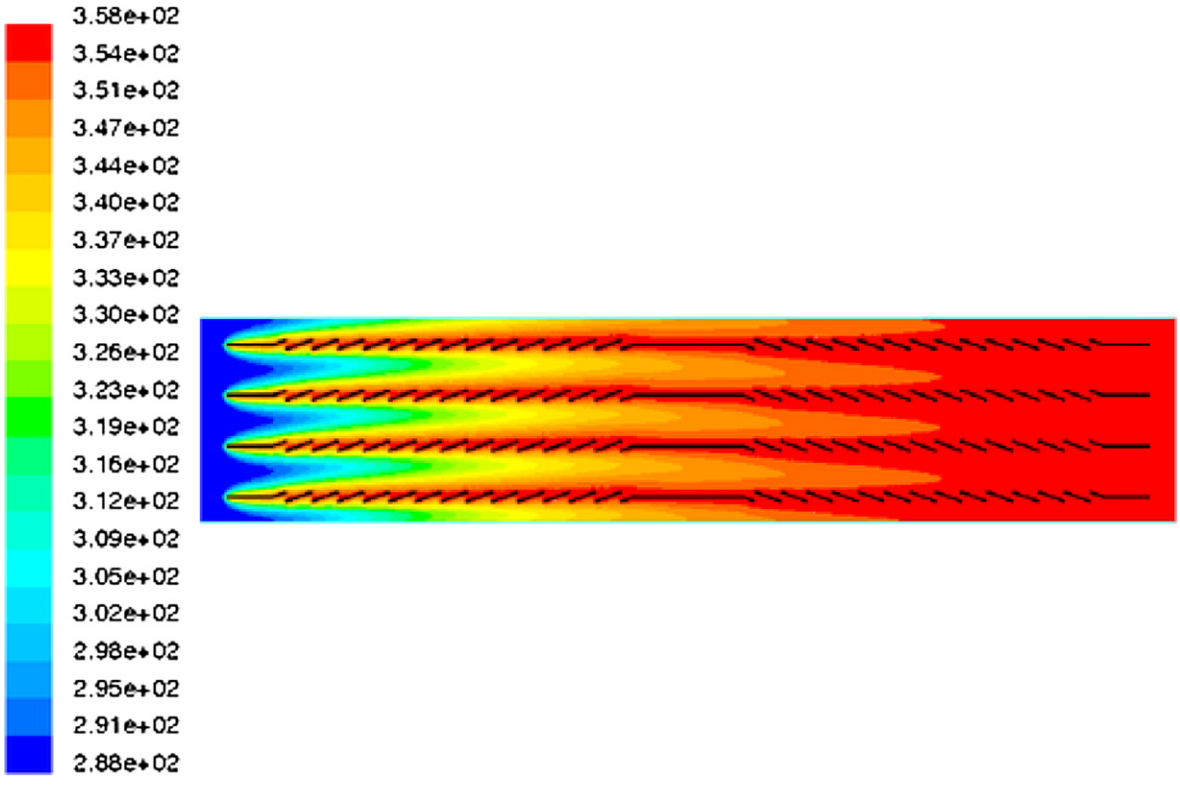

Fig. 5. Computed temperature (K) contours for $Re_d = 100$.

heat transfer. At higher Reynolds numbers, the boundary layers around the louvers are thinner and the flow is nearly aligned with the louvers. In this case temperature of air increases along the flow direction, and a significant temperature difference is maintained between air and fin. Hence the heat transfer rate is increased with Reynolds number,which is also discussed by

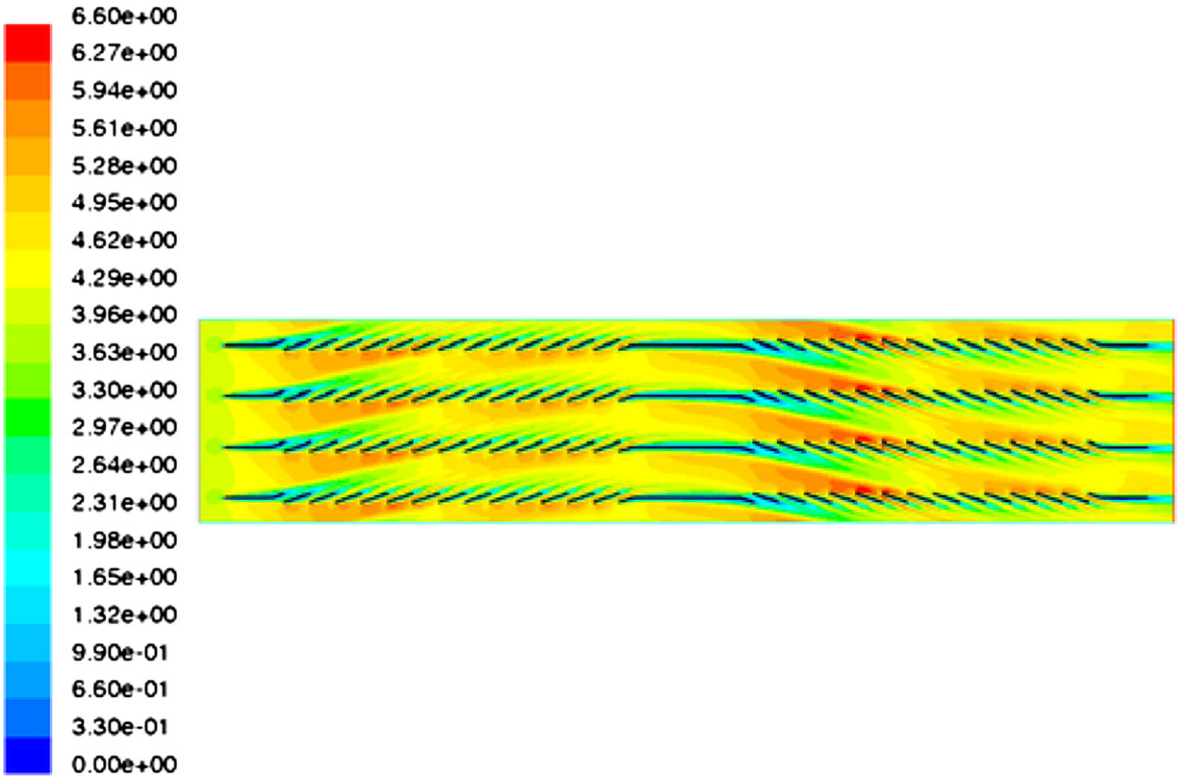

Fig. 6. Computed velocity ($\mathrm{m\,s^{-1}}$) contours for $Re_d = 1000$.

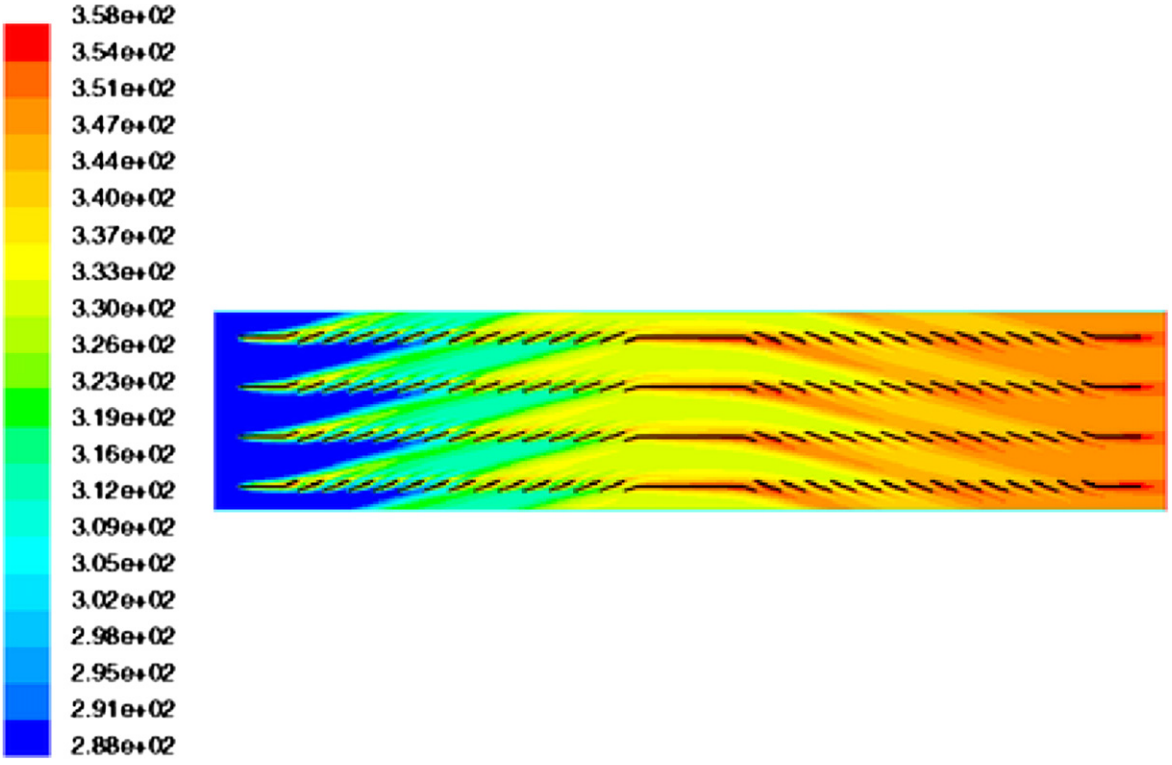

Fig. 7. Computed temperature (K) contours for $Re_d = 1000$.

Webb et. al. [11] in terms of flow efficiency. Fig. 8 shows the total pressure distribution across the louver. It can be seen that low pressure zone is formed near the louvers due to formation of boundary layer. The air which flows through the louver strikes on the flat plate and is turned. This flow diversion causes high pressure zone in the middle portion, as observed in Fig. 8.

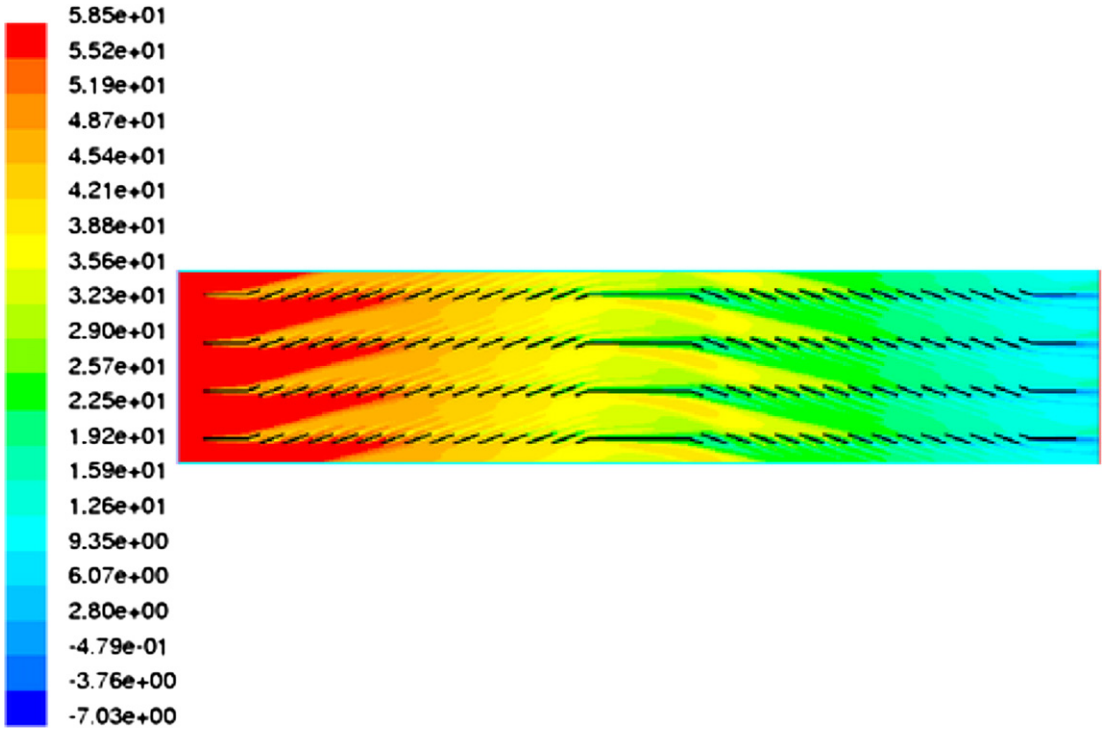

Fig. 8. Total pressure (pascal) contours across louvers for $Re_d = 1000$.

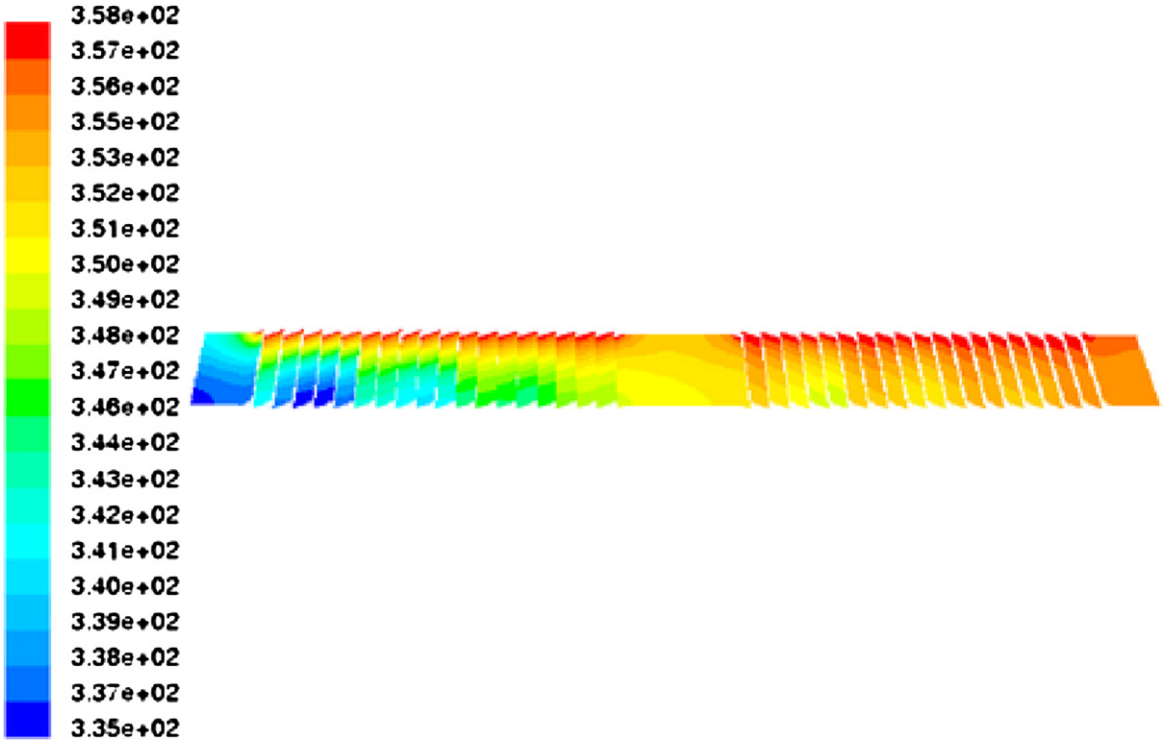

Fig. 9. Static temperature (K) contours on fins; $F_p = 1.72$ mm, $L_P = 0.81$ mm, $\alpha = 29°$, $T_p = 11$ mm, $Re_d = 1000$.

6.2. *Fin temperature distributions*

Figs. 9 and 10 show the typical static temperature contour on fin for Reynolds number Re_d = 1000 and 4000, respectively. It can be seen that the temperature of first two louvers are higher than adjacent four louvers. Similarly in the second half of fin, the temperature of first two louvers are higher than the adjacent louvers. This is due to the presence of a stationary vortex which

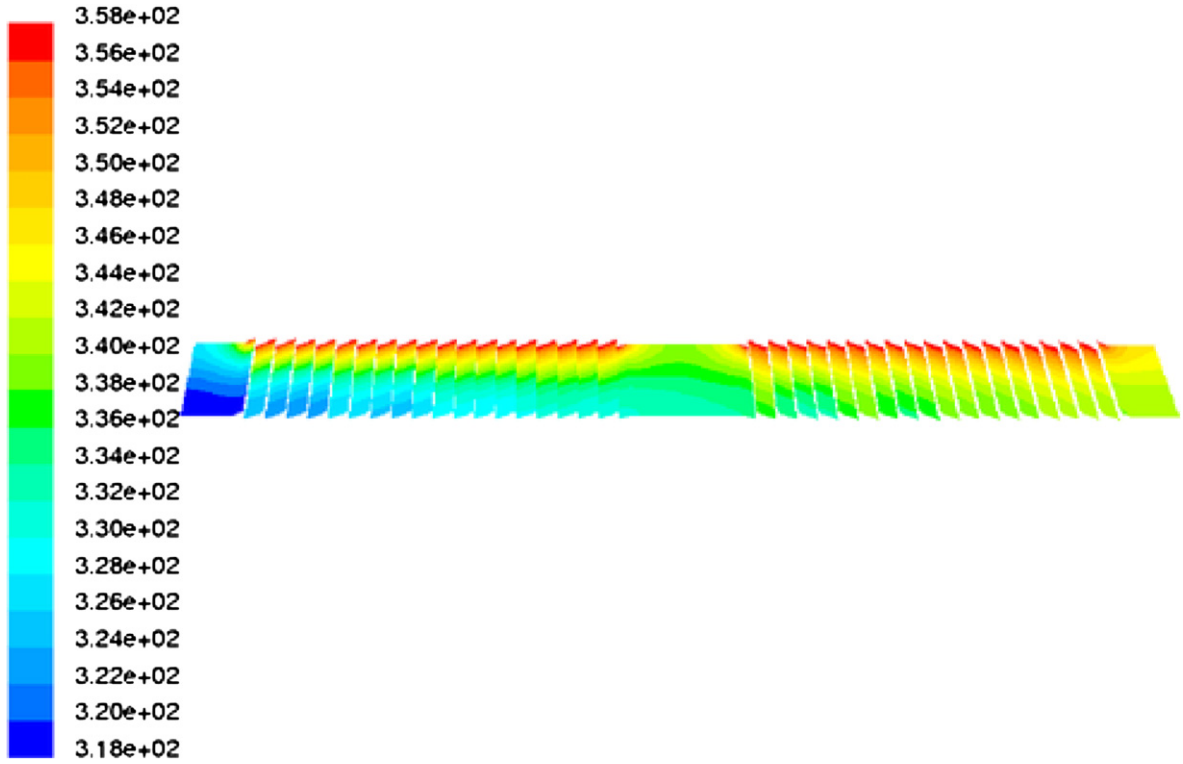

Fig. 10. Static temperature (K) contours on fins; $F_p = 1.72$ mm, $L_P = 0.81$ mm, $\alpha = 29°$, $T_p = 11$ mm, $Re_d = 4000$.

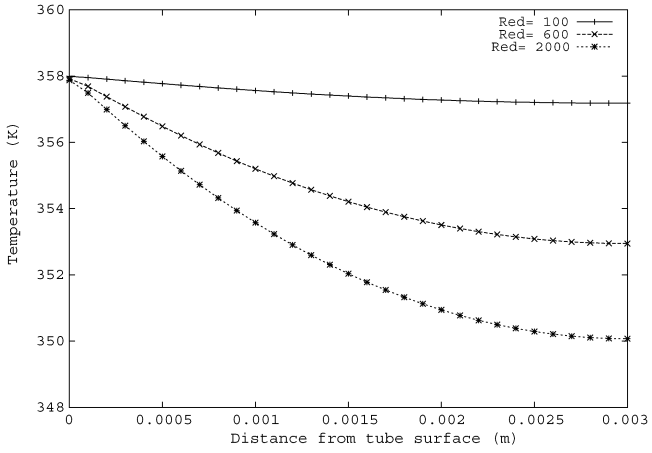

Fig. 11. Temperature variation across the fin at middle of upstream tube; $F_p = 2.17$ mm, $L_p = 1.1$ mm, $T_p = 8$ mm, $\alpha = 22°$.

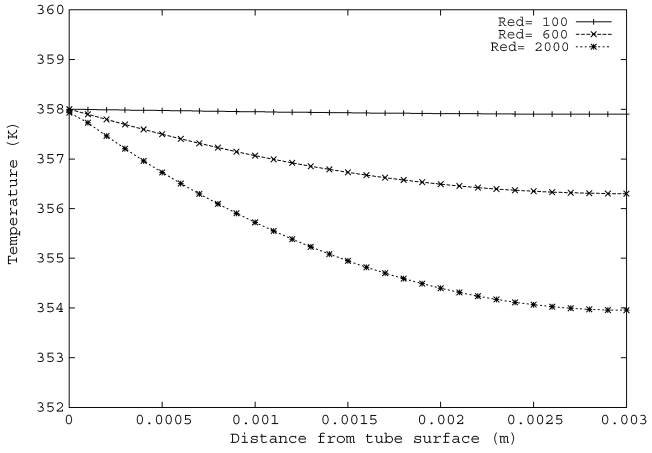

Fig. 12. Temperature variation across the fin at middle of downstream tube; $F_p = 2.17$ mm, $L_p = 1.1$ mm, $T_p = 8$ mm, $\alpha = 22°$.

develops between the first two louvers. This vortex blocks the airflow passage, and prevents the directing effect of the first two louvers. Temperature variation across the middle of the upstream and downstream of the fin is shown in Figs. 11 and 12. A similar trend is observed for all other configurations. It is found that the temperature of the fin decreases with the distance from the tube surface because of the thermal resistance of fin and the heat carried away by the cooling air. It is also found that the temperature at the symmetry of the fin falls further as pitch of the tube is increased. It is also observed that the temperature of fins falls as Reynolds number increases because of high heat transfer coefficient at large Reynolds number.

6.3. Heat transfer and pressure drop characteristics

Heat transfer and pressure drop characteristics are presented in terms of non-dimensional parameters, Stanton number (St) and friction factor (f). Figs. 13 and 14 show the computed and experimental values of Stanton number and friction factor as functions of Reynolds number for two configurations given in Table 1. The values of experimental and computed Stanton number and friction factors are given in Tables 2–5, respectively. It is to be noted that the experimental values are extracted from the work by Achaichia and Cowell [1]. Close agreement is found between the computational results and experimental

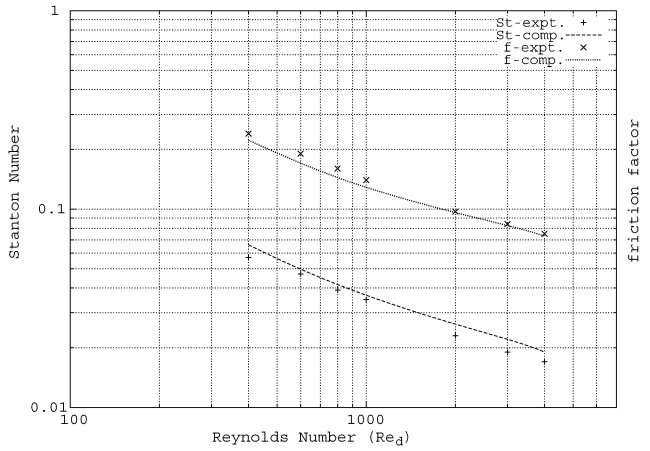

Fig. 13. Computed and experimental [1] Stanton number and friction factor for configuration 1.

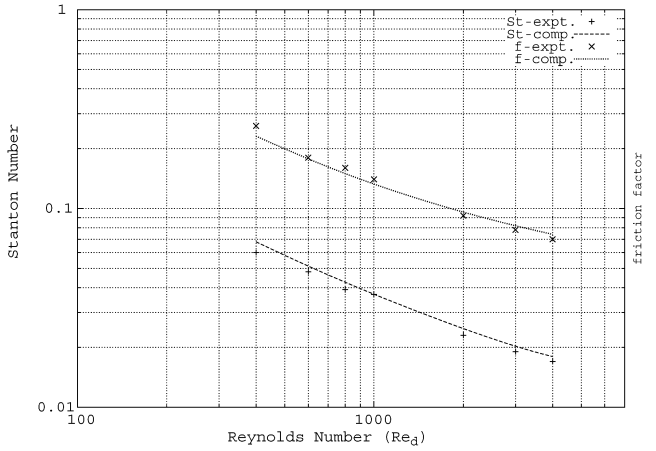

Fig. 14. Computed and experimental Stanton number and friction factor for configuration 5.

Table 2
Comparison of experimental and computed Stanton number; St_e = Stanton number experimental, St_c = Stanton number computed

Re_d	Configuration number															
	1		2		3		4		5		6		7		8	
	St_e	St_c	St_e	St_c	St_e	St_c	St_e	St_c	St_e	St_c	St_e	St_c	St_e	St_c	St_e	St_c
400	0.057	0.066	0.062	0.073	0.052	0.058	0.05	0.067	0.06	0.068	0.068	0.068	0.056	0.062	0.059	0.085
600	0.047	0.049	0.049	0.057	0.04	0.043	0.04	0.051	0.048	0.051	0.05	0.052	0.042	0.046	0.05	0.065
800	0.039	0.041	0.043	0.048	0.034	0.036	0.033	0.042	0.039	0.042	0.042	0.043	0.037	0.037	0.045	0.055
1000	0.035	0.036	0.038	0.043	0.029	0.031	0.029	0.037	0.037	0.0369	0.038	0.0375	0.032	0.032	0.04	0.049
2000	0.023	0.025	0.027	0.029	0.019	0.02	0.019	0.023	0.023	0.024	0.025	0.0239	0.023	0.019	0.028	0.032
3000	0.019	0.023	0.02	0.025	0.016	0.02	0.015	0.0189	0.019	0.02	0.02	0.022	0.019	0.024	0.021	0.029
4000	0.017	0.019	0.018	0.024	0.013	0.014	0.013	0.02	0.017	0.018	0.017	0.019	0.017	0.0198	0.019	0.024

Table 3
Comparison of experimental and computed Stanton number; St_e = Stanton number experimental, St_c = Stanton number computed

Re_d	Configuration number													
	9		10		11		12		13		14		15	
	St_e	St_c	St_e	St_c	St_e	St_c	St_e	St_c	St_e	St_c	St_e	St_c	St_e	St_c
400	0.061	0.084	0.033	0.049	0.062	0.078	0.049	0.066	0.062	0.071	0.068	0.074	0.05	0.07
600	0.052	0.062	0.038	0.062	0.05	0.06	0.048	0.055	0.051	0.055	0.055	0.06	0.045	0.055
800	0.043	0.052	0.039	0.051	0.043	0.05	0.043	0.049	0.045	0.046	0.047	0.05	0.039	0.045
1000	0.038	0.044	0.04	0.045	0.038	0.043	0.039	0.044	0.04	0.04	0.04	0.043	0.035	0.039
2000	0.024	0.029	0.03	0.031	0.025	0.028	0.028	0.031	0.025	0.035	0.026	0.0267	0.023	0.025
3000	0.02	0.027	0.023	0.028	0.021	0.025	0.02	0.025	0.02	0.027	0.02	0.026	0.019	0.23
4000	0.018	0.021	0.02	0.023	0.018	0.02	0.017	0.0209	0.018	0.022	0.07	0.079	0.017	0.21

Table 4
Comparison of experimental and computed friction factor; f_e = friction factor experimental, f_c = friction factor computed

Re_d	Configuration number															
	1		2		3		4		5		6		7		8	
	f_e	f_c	f_e	f_c	f_e	f_c	f_e	f_c	f_e	f_c	f_e	f_c	f_e	f_c	f_e	f_c
400	0.24	0.222	0.4	0.228	0.24	0.22	0.25	0.205	0.26	0.231	0.38	0.29	0.25	0.206	0.27	0.277
600	0.19	0.169	0.26	0.178	0.18	0.167	0.17	0.161	0.18	0.176	0.24	0.21	0.19	0.155	0.195	0.22
800	0.16	0.141	0.19	0.153	0.15	0.137	0.14	0.133	0.16	0.148	0.19	0.18	0.16	0.126	0.17	0.18
1000	0.14	0.124	0.16	0.137	0.13	0.118	0.12	0.116	0.14	0.129	0.16	0.13	0.13	0.113	0.15	0.16
2000	0.097	0.093	0.1	0.095	0.088	0.081	0.081	0.078	0.092	0.092	0.092	0.087	0.09	0.077	0.096	0.119
3000	0.084	0.085	0.082	0.088	0.075	0.081	0.07	0.0647	0.078	0.082	0.078	0.086	0.078	0.079	0.079	0.112
4000	0.075	0.073	0.076	0.083	0.068	0.082	0.064	0.066	0.07	0.074	0.07	0.078	0.07	0.068	0.07	0.097

Table 5
Comparison of experimental and computed friction factor; f_e = friction factor experimental, f_c = friction factor computed

Re_d	Configuration number													
	9		10		11		12		13		14		15	
	f_e	f_c	f_e	f_c	f_e	f_c	f_e	f_c	f_e	f_c	f_e	f_c	f_e	f_c
400	0.26	0.28	0.3	0.176	0.27	0.264	0.22	0.198	0.22	0.23	0.3	0.233	0.2	0.208
600	0.19	0.21	0.21	0.193	0.19	0.2	0.18	0.179	0.18	0.18	0.21	0.189	0.16	0.165
800	0.17	0.18	0.18	0.18	0.17	0.17	0.16	0.16	0.15	0.153	0.17	0.159	0.14	0.141
1000	0.15	0.16	0.16	0.16	0.14	0.15	0.14	0.14	0.13	0.135	0.15	0.139	0.12	0.122
2000	0.095	0.11	0.1	0.12	0.088	0.107	0.085	0.1	0.088	0.11	0.095	0.098	0.076	0.083
3000	0.08	0.091	0.082	0.1	0.07	0.09	0.07	0.086	0.072	0.089	0.078	0.085	0.063	0.071
4000	0.07	0.08	–	0.1	0.065	0.087	0.062	0.076	0.065	0.076	0.07	0.0787	0.059	0.067

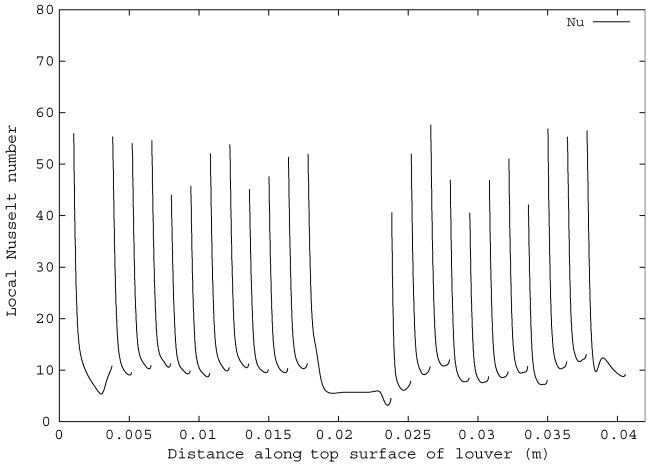

Fig. 15. Nusselt number along top surface of louver for $Re_d = 1000$.

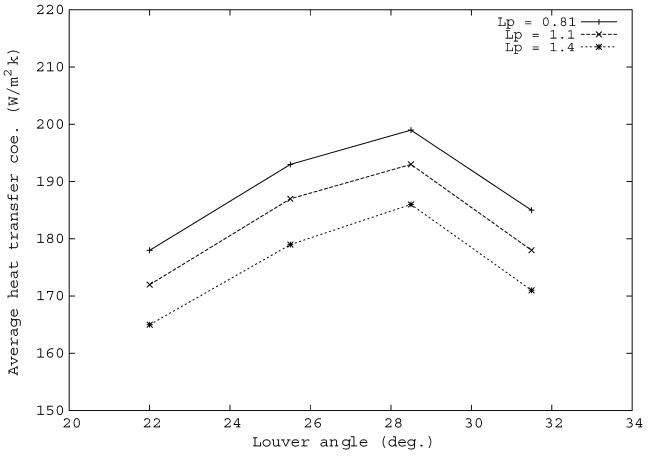

Fig. 16. Effect of louver angle (α) on heat transfer coefficient for $F_p = 2.17$ mm and $Re_d = 1000$.

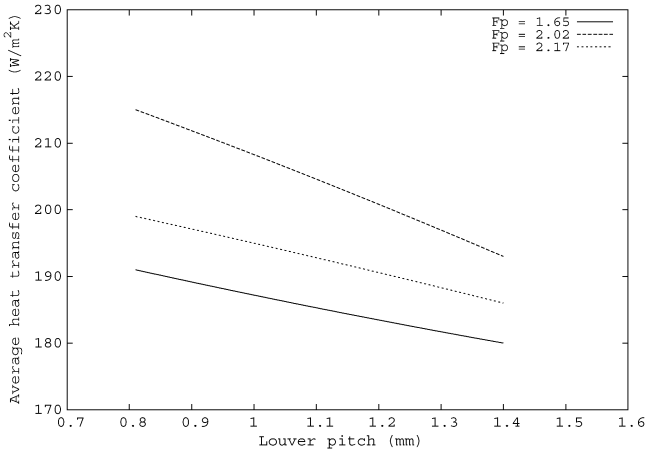

Fig. 17. Effect of louver pitch (L_p) on heat transfer coefficient for $\alpha = 28.5°$ and $Re_d = 1000$.

data at intermediate and high Reynolds number. However, at low Reynolds number there is a large deviation. This can be explained as follows. For low Re_d the flow is not louver directed, which results in the flow being not aligned with the mesh. This in turn causes some numerical false diffusion. Also, uncertainties in the experimental Stanton numbers and friction factors estimated by Achaichia and Cowell [1] have been reported to be 6.5% and 15%, respectively at low Reynolds number.

6.4. Local Nusselt number

The local Nusselt number on the top surface of each louver in the flow direction is calculated and plotted along the length of fin for Reynolds number $Re_d = 1000$ as shown in Fig. 15. It is observed that a high Nusselt number is obtained at the tip of the fin and leading edge of each louver. The Nusselt number is also high at the trailing edge of each louver. The Nusselt number falls rapidly over each louver before increasing slightly at the end of each louver. The increase in Nusselt number is due to flow impingement and local flow acceleration as the air enter the gap between the louver.

6.5. Effect of geometrical parameters

Performance of the louvered fin compact heat exchanger depends on the various geometrical parameters such as louver pitch (L_p), louver angle (α), fin pitch (F_p). Fig. 16 shows the effect of louver angle on heat transfer coefficient for fin pitch $F_p = 2.17$ mm. It can be observed that the heat transfer coefficient increases with louver angle and reaches maximum value at 28–29° and then again decreases with the increase in louver angle. This is because at higher Reynolds number, the flow is aligned with the louver at this angle. Fig. 17 shows the effect of louver pitch on heat transfer coefficient at optimum louver angle. Figs. 16 and 17 also show that higher heat transfer coef-

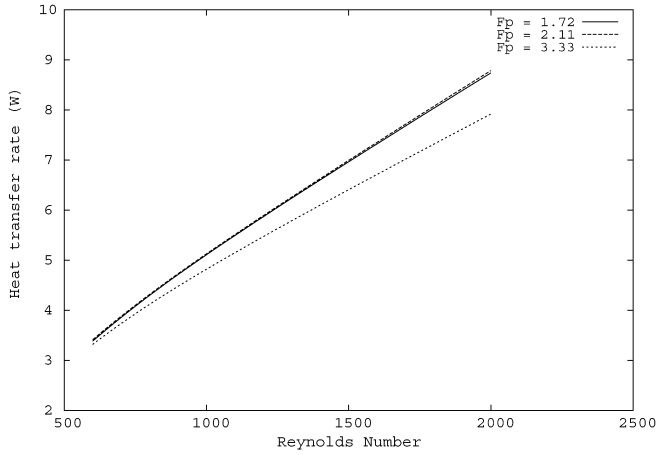

Fig. 18. Effect of fin pitch (F_p) on heat transfer rate for $L_p = 0.81$ mm, $T_p = 11$ mm and $\alpha = 29°$.

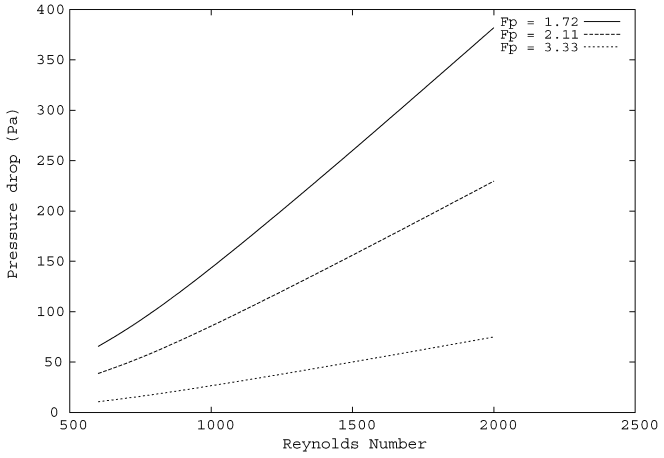

Fig. 19. Effect of fin pitch (F_p) on pressure drop for $L_p = 0.81$ mm, $T_p = 11$ mm and $\alpha = 29°$.

ficient is obtained at smaller louver pitch, i.e., $L_p = 0.81$ mm. The decrease in louver pitch causes the formation of a thin boundary layer which in turn interrupts the air flow. But below a certain value of the louver pitch, the pressure drop is large and hence $L_p = 0.81$ mm is considered to be the optimum louver pitch for this study. The effect of fin pitch on heat transfer rate and pressure drop are shown in Figs. 18 and 19, respectively. In Fig. 18 it is observed that by decreasing the fin pitch from 3.33 mm to 2.11 mm, heat transfer rate increases. However further reduction in fin pitch from 2.11 mm to 1.72 mm, does not result in any additional improvement in heat transfer. In Fig. 19, it can be observed that the pressure drop increases with decreasing fin pitch from 3.33 mm to 1.72 mm. This is because as the fin pitch is reduced, air flowing smoothly between the louvers can no longer pass easily and hence the full effect of louver is not obtained due to development of boundary layer and vortex formation. Therefore, it is important to select a suitable fin pitch to match the louver pitch for fluid flow along the louver. From this study it can be concluded that the configuration 8, which has heat transfer coefficient of 237 $\mathrm{W\,m^{-2}\,K^{-1}}$ and pressure drop of 81 Pa for $Re_d = 1000$, is the desired configuration with respect to maximum heat transfer for an allowable pressure drop. This configuration is having a louver pitch $L_p = 0.81$ mm, fin pitch $F_p = 2.11$ mm, lover angle $\alpha = 29°$ and tube pitch $T_p = 11$ mm.

7. Conclusions

Numerical simulation of a compact louvered fin heat exchangers is performed for the determination of heat transfer and pressure drop characteristics. Fifteen different configurations are studied here. Design curves are provided for air side heat transfer and pressure drop characteristics of finned heat exchanger. The simulation results are compared with experimental data. The computed Stanton numbers and friction factors are found to be in good agreement with the experiment except at low Reynolds number. It is found that at low Reynolds number the flow is fin directed and at higher Reynolds number the flow is louver directed. The local Nusselt number estimation suggests that Nusselt number is substantially high at the fin tip and at the leading and trailing edges of the louver. It is also found that both Stanton number and friction factor decrease with the increase in fin pitch. For any configuration there exists an optimal louver angle for which heat transfer coefficient is maximum. A parametric variation of the geometry provides a desired configuration for which the heat transfer coefficient is maximum and the pressure drop is within the allowable design limit.

References

[1] A. Achaichia, T.A. Cowell, Heat transfer and pressure drop characteristics of flat tube and louvered plate fin surfaces, Experimental Thermal and Fluid Science 1 (1998) 147–157.

[2] C.J. Davenport, Heat transfer and flow friction characteristics of louvered heat exchanger surfaces, in: J. Taborek, G.F. Hewitt, N. Afgan (Eds.), Heat Exchangers: Theory and Practice, Hemisphere/McGraw-Hill, Washington, DC, 1983, pp. 397–412.

[3] C.W. Bullard, M. Kim, Air-side thermal hydraulic performance of multi-louvered fin aluminum heat exchangers, Int. J. Refrigeration 25 (2002) 390–400.

[4] Y. Chang, C. Wang, W. Chang, Heat transfer and flow characteristics of automotive brazed aluminum heat exchangers, ASHRAE Transaction 100 (2) (1994) 643–652.

[5] Y. Chang, C. Wang, A generalized heat transfer correlation for louvered fin geometry, Int. J. Heat Transfer 40 (3) (1997) 533–544.

[6] C.C. Wang, C.J. Lee, C.T. Chang, S.P. Lin, Heat transfer and friction correlation for compact louvered fin-and-tube heat exchangers, Int. J. Heat Mass Transfer 42 (1999) 1945–1956.

[7] F.N. Beauvais, An aerodynamic look at automotive radiators, SAE Paper No. 650470, 1965.

[8] L.T. Wong, M.C. Smith, Airflow phenomenon in the louvered fin heat exchanger. SAE Paper No. 730237, 1973.

[9] A.A. Antoniou, M.R. Heikal, T.A. Cowell, Measurements of local velocity and turbulence levels in arrays of louvered plate fins, in: Proceedings of the Ninth International Heat Transfer Conference, Jerusalem, 1990, pp. 105–110.

[10] M. Kajino, M. Hiramatsu, Research and development of automotive heat exchangers, in: W.J. Wang, Y. Mori (Eds.), Heat Transfer in High Technology and Power Engineering, Hemisphere, Washington, DC, 1987, pp. 420–432.

[11] R.L. Webb, P. Trauger, Flow structured in the louvered fin heat exchanger geometry, Experimental Thermal and Fluid Science 4 (1991) 205–217.

[12] H. Aoki, T. Shinagawa, K.K. Suga, An experimental study of the local heat transfer characteristics in automotive louvered fins, Experimental Thermal and Fluid Science 2 (1989) 293–300.
[13] D.K. Tafti, G. Wang, W. Lin, Flow transition in a multilouvered fin array, Int. J. Heat Mass Transfer 43 (2000) 901–919.
[14] D.K. Tafti, X. Zhang, Geometry effects on flow transition in multilouvered fins-onset, propagation, and characteristics frequencies, Int. J. Heat Mass Transfer 44 (2001) 4195–4210.
[15] J. Cui, D.K. Tafti, Computations of flow and heat transfer in a three-dimensional multilouvered fin geometry, Int. J. Heat Mass Transfer 45 (2002) 5007–5023.
[16] D.K. Tafti, J. Cui, Fin-tube junction effects on flow and heat transfer in flat tube multilouvered heat exchangers, Int. J. Heat Mass Transfer 46 (2003) 2027–2038.
[17] T. Perrotin, D. Clodic, Thermal-hydraulic CFD study in louvered fin-and-flat-tube heat exchangers, Int. J. Refrigeration 27 (2004) 422–432.
[18] K.N. Atkinson, R. Drakulic, M.R. Heikal, T.A. Cowell, Two- and three-dimensional numerical models of flow and heat transfer over louvered fin arrays in compact heat exchangers, Int. J. Heat Mass Transfer 41 (1998) 4063–4080.
[19] S.J. Baldwin, P.R.S. White, A.J. Al-Daini, Investigation of the gas side flow field in multilouvered ducts with flow reversal, in: Proceedings of the Fifth International Conference on Numerical Methods in Laminar and Turbulent Flow, Montreal, 1987, pp. 482–495.
[20] Y. Yuan, A. Jackson, M. Nelson, CFD simulation of flow and heat transfer in airways, SAE Paper, 2001-01-1712, 2001.
[21] M.E. Springer, K.A. Thole, Experimental design for flowfield studies of louvered fins, Experimental Thermal and Fluid Science 18 (1998) 258–269.
[22] D.K. Tafti, L.W. Zhang, G. Wang, Time-dependent calculation procedure for fully developed and developing flow and heat transfer in louvered fin geometries, Numerical Heat Transfer Part A 35 (1999) 225–249.
[23] FLUENT, User's Guide, Release 6.1, Fluent Inc., Lebanon, New Hampshire.
[24] S.V. Patankar, Numerical Heat Transfer and Fluid Flow, Hemisphere, London, 1980.
[25] H.K. Versteeg, W. Malalsekara, An Introduction to Computational Fluid Dynamics – The Finite Volume Method, Prentice-Hall, New York, 1995.
[26] W.M. Kays, A.L. London, Compact Heat Exchangers, second ed., McGraw-Hill, New York, 1984.